# Effect of membrane thickness on hydrogen permeation in steels during wet H2S exposure

J. Kittel, F. Ropital, J. Pellier

# EFFECT OF MEMBRANE THICKNESS ON HYDROGEN PERMEATION IN STEELS DURING WET $H_2S$ EXPOSURE

J. Kittel, F. Ropital, J. Pellier

IFP-Lyon

Rond-point de l'échangeur de Solaize - BP3

69360, Solaize (FRANCE)

## ABSTRACT

The permeation of hydrogen in steel in the presence of acid gases is not a simple phenomenon as the steel may contain trapping sites and also because the permeation may be governed by surface reactions associated with corrosion. Recently, hydrogen permeation experiments carried out at the corrosion potential have shown a constant flux for various membrane thicknesses in the range 0.05 – 0.8 mm. These results revealed the difficulty to express the flux for thicker steel membrane (i.e. pipe) from laboratory studies on thin membranes, as the classical rule (flux proportional to the inverse of the membrane thickness) is not always applicable and not conservative.

This paper presents new permeation results, obtained on steel membranes up to 10 mm thick. The transition between thin and thick membranes is clearly established, and is in the millimeter range in sour conditions. The necessity to adopt a new interpretative framework to link permeation measurements and hydrogen cracking mechanisms is reinforced. For thin membranes, the permeation flux is constant and governed only by the charging flux crossing the entry face. This surface mechanism is probably correlated with surface cracking mode, like SSC.

On the other hand, the traditional concept of diffusion can only be used in thick membrane situations. The diffusion flux is inversely proportional to the sub-surface concentration. This concentration is in direct relation with the hydrogen activity in the steel, which is probably correlated with internal cracking modes, like HIC.

**Keywords**: Hydrogen permeation, $H_2S$, Hydrogen embrittlement, HIC, SSC

## INTRODUCTION

Hydrogen damage is one of the major causes of steel equipment failures in the oil & gas industry[1-7]. It is caused by the dissolution of hydrogen in the steel, as a result of the cathodic reduction of $H^+$ which accompanies the anodic oxidation of iron in acid media. The reduction of water molecules by cathodic overprotection is another potential source of reduced $H^+$. Several failure modes can occur in service, for example:

- hydrogen induced cracking (HIC), corresponding to internal cracks generated by the recombination of hydrogen to gaseous molecules at certain appropriate traps in the steel, like MnS inclusions of pearlite bands. This failure mode is strictly internal, and does not require an external stress[2,8-15].
- Hydrogen stress cracking (HSC), also designed as sulfide stress cracking (SSC) when H2S is present: this cracking mode is generated from the surface of the steel and requires an applied stress[16-24].

The presence of $H_2S$ is known to have an aggravating influence.

In this respect, measurement of hydrogen permeation through steel membranes is an interesting technique, as it allows the determination of some important parameters like the diffusion coefficient and the hydrogen concentration in the metal[20,21,25-33].

Another issue of hydrogen permeation through steels was recently discussed for pipe-in-pipe applications[34]. Pipe-in-pipe structures might be used when thermal insulation is required to assure flow. In such systems, the production fluid is transported in the internal pipe. The thermal barrier is achieved by a vacuum or insulating material in the annular space between the internal and external pipe. Then, if hydrogen permeates through the steel and enters the annulus, the thermal efficiency might be lost.

**Hydrogen Permeation and Hydrogen Cracking Susceptibility**

Hydrogen permeation measurements have long been used as an experimental method for the assessment of hydrogen cracking mechanisms, and especially through the determination of the concentration of dissolved hydrogen. Many authors have used electrochemical permeation measurements for laboratory evaluation of steel susceptibility to all forms of hydrogen induced cracking, either HIC[25,27] or SSC[16,17,20,21,32,33,35]. Other studies even used hydrogen permeation as a unique experimental technique, for comparing different thermal treatments[36,37] for martensitic low carbon steels. More academic studies also used different permeation techniques for a discussion of sour environments severity towards HIC or SSC[38].

More recently, on-site monitoring by an air stream measurement device[39] has also been made available. This apparatus has been applied on-site for the evaluation of refinery equipment[40,41] pressure vessels[42] or for wet sour gas pipelines[43]. It was also used for laboratory studies on thick steel membranes[44-46].

The modeling of hydrogen permeation data usually considers an adsorption step from the solution to the metal surface, followed by an absorption in the bulk metal[28,47-50]. The first reaction to be considered is the adsorption of hydrogen at the metal surface (Volmer reaction):

$$H^{+}_{(aq)} + e^{-}_{(M)} \rightarrow H_{ads} \quad (1)$$

where $H^{+}_{(aq)}$ represents a hydrated proton, $e^{-}_{(M)}$ an electron usually supplied by the metal M, and $H_{ads}$ represents a hydrogen atom adsorbed at the surface.

Once adsorbed, $H_{ads}$ can either recombine to molecular hydrogen ($H_2$), or be transferred from an adsorbed state at the surface to an absorbed state in the bulk metal. Recombination can occur following the Tafel (Equation 2) or Heyrowsky (Equation 3) reactions:

$$H_{ads} + H_{ads} \rightarrow H_2 \quad (2)$$

$$H_{ads} + H^{+}_{(aq)} + e^{-}_{(M)} \rightarrow H_2 \quad (3)$$

The surface – bulk transfer can be written as:

$$H_{ads} \rightarrow H_{abs} \quad (4)$$

The rates of this reaction depend mainly on the surface coverage by adsorbed hydrogen ($H_{ads}$) and on the subsurface concentration of absorbed hydrogen ($H_{abs}$). Once absorbed in the sub-surface $H_{abs}$ can diffuse in the metal.

Most of the aforementioned studies on HIC or SSC were made with the assumption that the Fick's laws of diffusion can be applied. Considering one-dimensional diffusion though a membrane of thickness $L$, the diffusion coefficient of hydrogen in steel can be determined from the analysis of the permeation transients $J(t)$. Under these conditions, the ratio between the permeation transient $J(t)$ and the steady-state flux $J_{ss}$ corresponding to the second Fick's law depends on the diffusion coefficient $D$ and on the membrane thickness $L$ [51,52]:

$$\frac{J(t)}{J_{ss}} = 1 + 2\sum_{n=1}^{\infty}(-1)^n \exp\left(-n^2\pi^2 \frac{D \times t}{L^2}\right) \quad (5)$$

The diffusion coefficient may then be calculated from the transient curve using for example the time lag method ($t_{lag}$ corresponds to the time at $J(t)/J_{ss} = 0.63$):

$$D = \frac{L^2}{6 \times t_{lag}} \quad (6)$$

Another method of calculation is based on the breakthrough time ($t_b$) corresponding to the elapsed time measured by extrapolation of the linear portion of the rising transient to $J(t) = 0$:

$$D = \frac{L^2}{15.3 \times t_b} \quad (7)$$

Many other methods have been described elsewhere[51,52].

Once the steady-state is reached, the hydrogen sub-surface concentration at the entry face $C$ can be determined with the first Fick's law of diffusion from $J_{ss}$ and the diffusion coefficient $D$:

$$J_{ss} = D \times C/L \quad (8)$$

However, this steady state situation strongly depends on the boundary conditions of the system and on the rate determining steps. The main cases are illustrated for a metal membrane with

one face in contact with the test solution. Only the steady state permeation is considered, and the trapping is neglected. Then, the path between $H_{ads}$ at the entry face and the extracted $H$ at the exit face can be described by four main fluxes (Figure 1):

- $J_{ch}$, the charging flux at the entry face, corresponding to the transfer from the adsorbed to absorbed state,

- $J_{\deg}$, the degassing flux at the entry face, corresponding to the transfer from absorbed to adsorbed state,

- $J_{diff}$, the diffusion in the bulk metal from the entry face to the exit face,

- $J_{ss}$, the net steady-state extraction flux at the exit face, corresponding to the balance between surface – bulk transfer and bulk – surface transfer at the exit face. The steady-state extraction flux could either correspond to physical degassing ($J_v$) for permeation measurements in vacuum or air, or to anodic extraction flux ($J_a$) for electrochemical measurements.

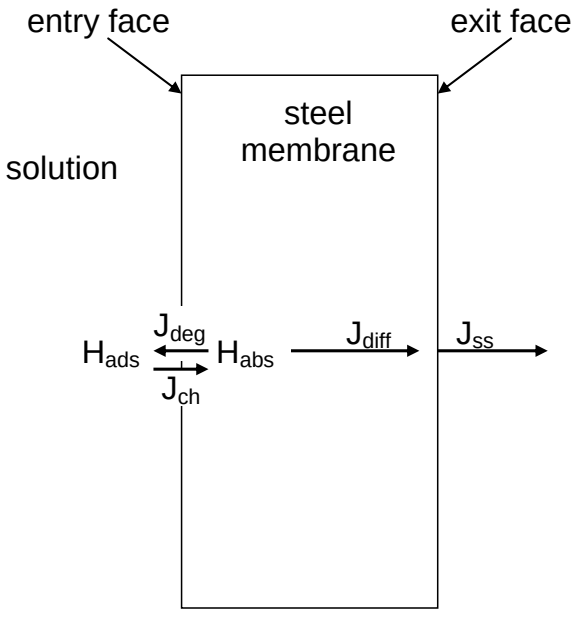


Figure 1: Different hydrogen fluxes through a steel membrane.

Considering that the extraction is ideal, the mass balance at the entry and exit faces gives:

$$J_{ss} = J_{diff} = J_{ch} - J_{\deg} \tag{9}$$

Then, two main cases are distinguished, depending on the conditions at the entry and exit faces of the specimen[38,53-55]:

1. If there is no concentration gradient, there is no driving force for diffusion in the bulk metal. Then the diffusion flux $J_{diff}$ in the bulk is zero. From Equation (9), we obtain:

$$J_{ss} = J_{diff} = 0 \tag{10}$$

$$J_{ch} = J_{\deg} \tag{11}$$

   The concentration of dissolved hydrogen is the same in the whole sample, and is equal to the sub-surface concentration $C_0$, which is governed by the surface – bulk equilibrium at the entry face.

2. If the concentration at the exit face is fixed to zero by an appropriate extraction method, a concentration gradient is established through the membrane giving rise to diffusion of $H$ in the metal. This is the practical case of most of the experimental studies of hydrogen permeation. Two limiting cases can be considered, depending on the relative values of

$J_{diff}$ , $J_{ch}$ and $J_{\deg}$ . According to Protopopoff and Marcus[50], if the membrane is thick or the diffusion coefficient $D$ is low, the permeation rate is limited by the diffusion rate in the bulk metal. Then:

$$J_{diff} \ll J_{ch} \approx J_{\deg} \tag{12}$$

The surface – bulk transfer rates $J_{ch}$ and $J_{\deg}$ are in quasi-equilibrium, and the hydrogen subsurface concentration $C_0$ is the same than in the first situation. Then, the diffusion flux is inversely proportional to the membrane thickness:

$$J_{diff} = D \times C_0 / L \tag{13}$$

This situation is described by Crolet and co-worker[38,53-55] as a "thick membrane" case, for which the sub-surface concentration $C_0$ does not depend on the membrane thickness. In such conditions, the experimental value of $C_0$ can be extrapolated to any membrane of the same steel exposed to the same solution, and the diffusion flux can be calculated from the new membrane thickness.

On the other hand, from equation (13), we can see that the decrease of the membrane thickness (or an increase of the diffusion coefficient) induces an increase of the diffusion flux $J_{diff}$ . For sufficiently thin membranes, $J_{diff}$ is no longer negligible towards $J_{ch}$ and $J_{\deg}$ and a new limiting case replaces Equation (12):

$$J_{diff} \approx J_{ch} >> J_{\deg} \quad (14)$$

The rate determining step is no longer the diffusion in the bulk metal, but the rate of hydrogen entry ($J_{ch}$). As a result, the diffusion flux $J_{diff}$ becomes independent of the membrane thickness. Similarly, the hydrogen sub-surface concentration $C^*$ is no more governed by the surface – bulk equilibrium at the entry face, but rather by the diffusion in the metal:

$$C^* = J_{diff} \times L/D = J_{ch} \times L/D < C_0 \quad (15)$$

This situation is described by Crolet and co-workers[38,53-55] as a "thin membrane" case, for which the diffusion flux is constant and does not depend on the membrane thickness. In such conditions, the value of the hydrogen sub-surface concentration $C^*$ can not be extrapolated to thicker membranes.

According to this model, the hydrogen sub-surface concentration and the diffusion flux follow two parallel but opposite evolutions with the test membrane thickness (Figure 2):

- below the critical thickness, in a thin membrane situation, the sub-surface concentration of hydrogen is proportional to the thickness, and the diffusion flux is constant,
- above the critical thickness, in a thick membrane situation, the sub-surface concentration is constant and the diffusion flux is inversely proportional with the thickness.

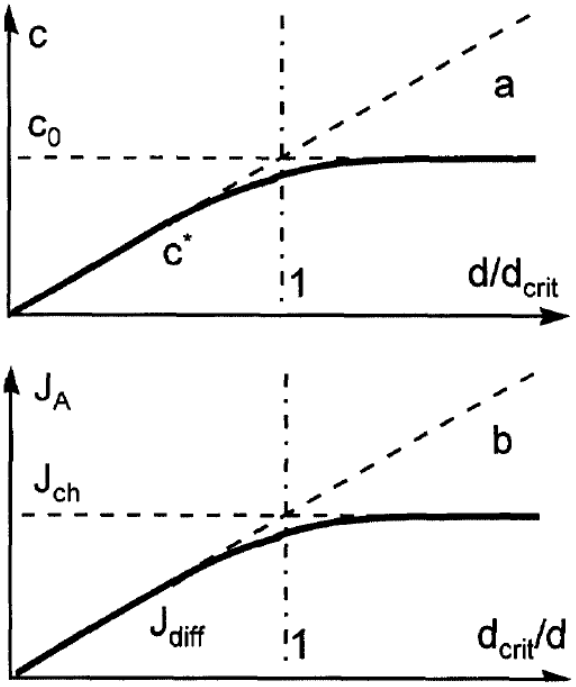


Figure 2: Evolution of (a) the hydrogen sub-surface concentration C, and (b) the permeation flux $J_A$ as a function of the normalized membrane thickness d / $d_{crit}$ (from ref. 54).

From the practical point of view, permeation measurements on thick membranes only allow an accurate determination of the hydrogen concentration in the steel at equilibrium. For the studies of internal hydrogen effects, such as HIC, measurements on thick membranes are necessary. On the other hand, permeation measurements on thin membranes are useful for the determination of the charging flux $J_{ch}$ crossing the entry face. Therefore, external hydrogen effects, such as SSC, which are controlled by the raw charging flux $J_{ch}$ crossing the entry face, should be evaluated with the aid of permeation measurements through thin membranes.

Unfortunately, the critical thickness ($d_{crit}$) where the transition between thin and thick membrane situation arise is not universal, but depends on the environment (pH, $pH_2S$, polarization...) and

also on the metal properties. It is therefore important to have an idea of the critical thickness for given steel and given environment.

For permeation studies in sulfuric acid or acetate buffer solutions and under potentiostatic or galvanostatic charging conditions, steady-state permeation fluxes proportional to the reciprocal of the membrane thickness were observed down to 0.01 mm thin steel membranes[28].
On the other hand, recent permeation measurements in $H_2S$ containing solutions revealed a thin membrane behavior for steel membranes up to 2 mm[34,38,54,55].

Therefore, the interpretation of permeation data in sour service conditions needs to be taken with great caution when measurements are made through 0.5 to 2.0 mm membranes, which might often behave like a thin membrane. In such conditions, the diffusion flux is constant and the subsurface concentration is proportional to the membrane thickness. Thus, it would be erroneous to extrapolate the hydrogen subsurface concentration to thicker membranes. At least, for experiments in sour conditions, it is recommended to check that the thick membrane behavior applies, i.e. that the permeation current is inversely proportional with the membrane thickness. It is only under this condition that the hydrogen sub-surface concentration determined from the first Fick's law is meaningful and available for extrapolation to thicker membranes. Unfortunately, the verification of this property is only rarely found in published papers[45].

The purpose of this paper is to investigate more closely the impact of steel membrane thickness on hydrogen permeation in sour environments. When $H_2S$ is present in the charging solution, recent papers revealed that hydrogen diffusion through the bulk steel might not be rate limiting, even for relatively thick steel membranes. These findings have important consequences for the transfer of laboratory results on thin membranes to the real industrial situation of thick steel pipelines or pressure vessels. The goals of the present experimental study were to clarify the

hydrogen permeation regimes in low alloyed steels exposed to sour conditions, and to discuss the practical consequences for HIC and SSC.

## EXPERIMENTAL PROCEDURES

### Tested Materials

Two different API X65 steels were selected for the experimental program. The first one was a sweet service LSAW pipe, 42 inches diameter and 1 inch (25.4 mm) thick. The second one was a sour service hot rolled plate, 20 mm thick. Their microstructures are compared in Figure 3 and Figure 4 respectively. Their chemical composition is given in Table 1. For each of the steels studied, the microstructure consisted mainly of ferrite with a portion of pearlite. The sweet service grade had a more pronounced banded structure, particularly pronounced in the mid-thickness. However, for all the permeation tests made during this study, no HIC was observed by ultrasonic inspection after immersion. Permeation membranes 70 x 70 mm² were machined from the raw materials, with thickness varying between 0.5 and 10 mm.

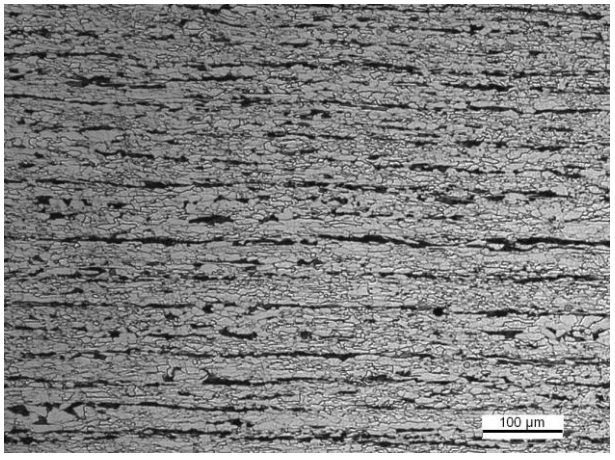


Figure 3: microstructure of the sweet service grade in the L direction.

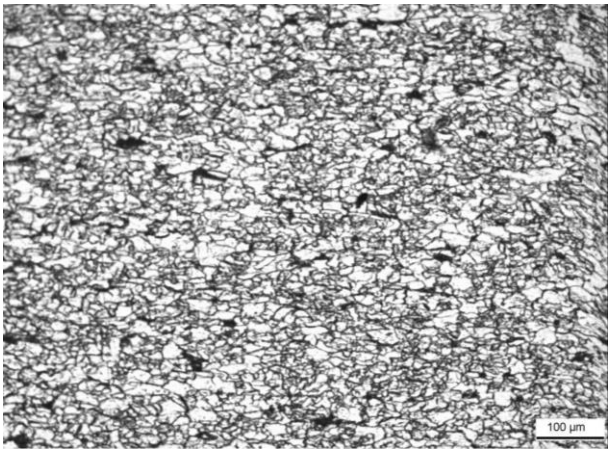


Figure 4: microstructure of the sour service grade in the L direction.

Table 1: chemical composition of tested steels (wt. %).

| | C | Mn | Si | P | S | Cr | Ni | Mo | Cu | Al | Ti | Nb |
|---|---|---|---|---|---|---|---|---|---|---|---|---|
| **steel A** | 0,046 | 1,36 | 0,322 | 0,008 | 0,001 | 0,041 | 0,036 | 0,008 | 0,047 | 0,036 | 0,019 | 0,045 |
| **steel B** | 0,09 | 1,56 | 0,28 | 0,014 | 0,001 | 0,05 | 0,03 | 0,01 | 0,02 | 0,030 | 0,000 | 0,040 |

**Corrosive medium**

All solutions were prepared according to EFC16 document[56], solution A, and thus contained 5% sodium chloride and 0.4% sodium acetate.

The bubbling gas is either pure $H_2S$, or a mixture of $CO_2$ with 0.3 % to 10 % $H_2S$, in order to obtain $H_2S$ partial pressure of 3 to 1000 mbar.

After a thorough deoxygenating step, the solution was saturated by bubbling gas at ambient pressure. The pH was then adjusted to desired level through addition of deaerated 1N hydrochloric acid or deaerated 1N sodium hydroxide NaOH. The solution was then poured into

the charging chamber. When the permeation current was stable, or after a period of 24 hours, the pH was decreased. Most of the time, the experimental sequence consisted of three pH steps: 5.5 – 4.5 – 3.5. For some specific tests, the experimental cell was place in an autoclave, in order to examine the impact of temperature. Some experiments at pH 3.5 were then done at 25, 40 and 55 °C.

**Permeation measurements: electrochemical / air stream**

Most of the permeation experiments were conducted with a Devanathan-Stachurski[28] cell (Figure 5) that was designed specially for thick specimens. The exposed surface area was 19.6 $cm^2$. The thickness of the specimen varied between 0.5 and 10 mm.

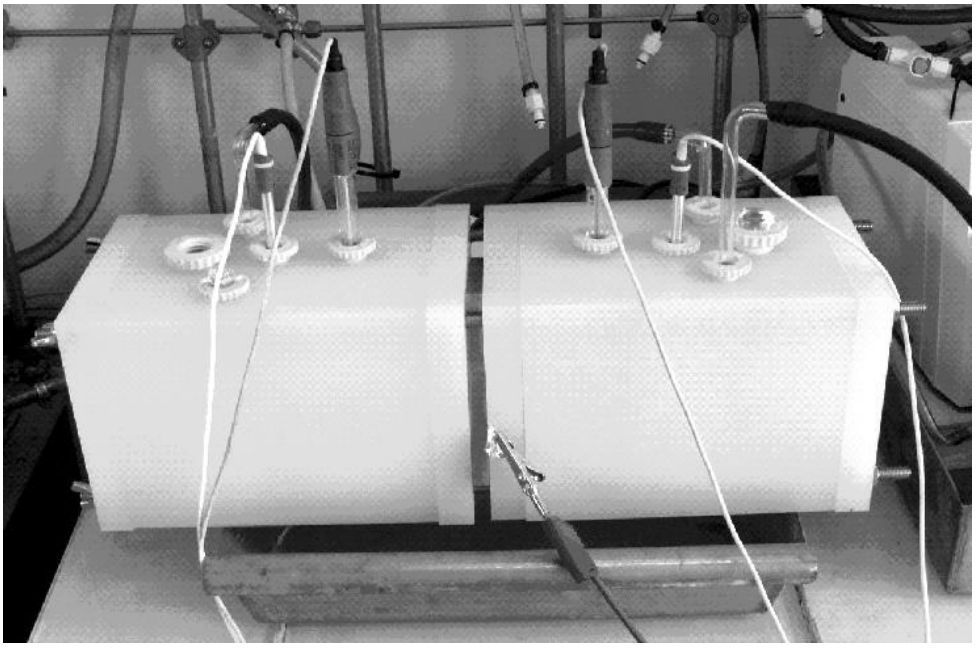

Figure 5: Devanathan-Stachurski cell for permeation measurements on thick specimens.

The experimental set-up consisted of two identical electrolytic cells separated by the steel membrane. The charging surface was left at the corrosion potential. The exit surface was coated with Pd[57-59] and held in a 0.1 M NaOH solution at a potential of +300 mV vs. the saturated calomel electrode (SCE). Thus all the hydrogen atoms diffusing through the membrane were oxidized, this oxidation current providing a measure of the hydrogen permeation flux.

Some experiments were made using the air stream measurement technique, with a device developed for industrial site monitoring[39,43]. The charging cell was identical to the one used for the electrochemical permeation, but the detection cell was replaced by a collector plate connected to the measurement apparatus. Under this configuration, the exit surface was simply rinsed with ethanol and dried. No palladium coating was used.

**Corrosion measurements: charging side**

For some tests, the corrosion rate of the steel in the charging solution was evaluated through polarization resistance ($R_p$) measurements. The experimental parameters were as follows:

- measurement of the open current potential ($E_{oc}$ vs. saturated calomel electrode) for 30 seconds,
- potentiondynamic sweep from -25 mV/ $E_{oc}$ to +25 mV/ $E_{oc}$ at 1 mV/s
- $R_p$ measurement by linear regression between -10 mV/ $E_{oc}$ to +10 mV/ $E_{oc}$

The corrosion current was then calculated using the Stern and Geary equation:

$$J_{corr} = \frac{1}{2.3} \times \frac{b_a \times b_c}{b_a + b_c} \times \frac{1}{R_p} \qquad (16)$$

In $H_2S$ containing solutions, previous studies[34,60] determined anodic slopes $b_a$ between 95 and 135 mV/decade, and $b_c$ between 180 and 270 mV/decade. For this study, we used 120 mV/decade for both the anodic and cathodic slopes.

The $R_p$ measurements were made at different exposure times. A rapid decrease was usually observed immediately after immersion, but it usually stabilized after several hours. Only the steady-state values were used for this study.

## RESULTS

### Comparisons of electrochemical and air stream techniques

According to Crolet and Bonis comparing different permeation techniques, air stream measurements are believed to provide a greater stability than electrochemical permeation[38]. It was shown that the extraction efficiency of their Pd coating was drastically decreased after one day of experiment. Therefore, these authors recommended that electrochemical methods should not be used for long term permeation studies.

In order to check the impact of the permeation flux measurement method, electrochemical and air stream techniques were compared during the same experiment. It was then possible to compare for two identical steel specimens submitted to the same charging solution:

- the electrochemical permeation rate $J_{electroch}$ related to the oxidation of $H$ into $H^+$ in a 0.1N NaOH solution and through a Pd coating,

- the air stream measurement $J_{airstream}$ related to the volume of $H_2$ effused from the exit face.

For the sake of comparison, the proportionality between the electrochemical ($J_{electroch}$) and the air stream ($J_{airstream}$) fluxes is given by:

$$J_{airstream}\left(L \cdot cm^{-2} \cdot s^{-1}\right) = K \times J_{electroch}\left(A \cdot cm^{-2}\right) \quad (17)$$

where $K$ is a proportionality coefficient given by:

$$K = \frac{1}{n \cdot F} \times \frac{R \cdot T}{P} \quad (18)$$

and $n$ is the number of electrons implied in the oxidation reaction (electrochemical measurement) corresponding to one molecule of $H_2$ in the case of gaseous recombination (air stream measurement), $F$ is the Faraday constant (96490 C/equiv.), $R$ is the universal gas constant (8.3143 J.mol$^{-1}$.K$^{-1}$), $T$ is the absolute temperature (K) and $P$ is the pressure (Pa). Then, at ambient temperature and pressure, we can calculate that $K = 127\, pL.\mu A^{-1}$.

Comparison between both extraction methods was made at ambient temperature on two membranes of steel B (10 mm) exposed to the test solution saturated with 1 bar $H_2S$ and at pH 4.5. The first membrane was used for electrochemical extraction with a standard Devanathan-Stachurski[28] arrangement, while an air stream hydrogen collector was placed on the second

membrane. The results are presented in Figure 6, for which the proportionality between the Y-scales was calculated with Equation (17) using $K = 127\, pL.\mu A^{-1}$.

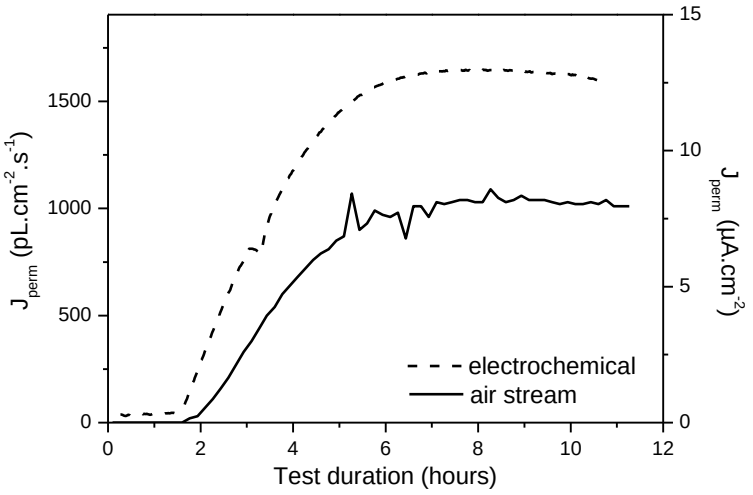


Figure 6: permeation transients measured simultaneously by air stream technique and electrochemical method, for two identical membranes (10 mm) of steel B exposed to test solution saturated with 1 bar $H_2S$ at pH 4.5.

Similar trends can be seen with both measurement techniques. However, the air stream method seems to give lower values. Indeed, when the steady-state flux is reached, the permeation flux measured by electrochemical extraction is 13 µA.cm$^{-2}$. According to Equation (17), the corresponding air stream flux would be 1650 pL.cm$^{-2}$.s$^{-1}$, while the flux effectively measured was only 1000 pL.cm$^{-2}$.s$^{-1}$.

This indicates that natural extraction in gas phase (as with the air stream collection method) is less efficient than extraction by electrochemical oxidation. A possible explanation is that the hydrogen sub-surface concentration at the exit face is not zero in the case of air stream extraction.

More comparative experiments should be necessary to examine this in more detail.

For the remaining part of this study, all the experiments were performed with the electrochemical method. As illustrated in Figure 7 a good stability of the electrochemical measurements for exposure times up to 100 hours was observed during our experiments.

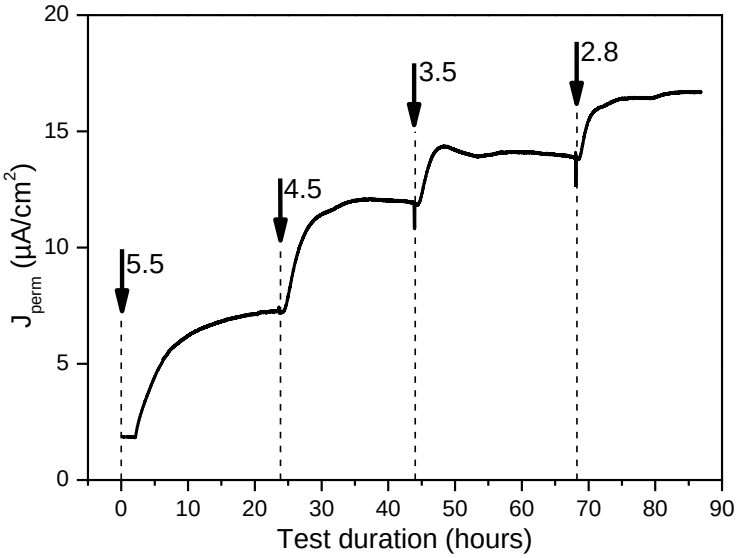


Figure 7: Permeation transient measured for a 10 mm membrane of steel B exposed to test solution at various pH saturated under 100 mbar $H_2S$ and 900 mbar $CO_2$.

**Impact of $pH_2S$ and pH**

The impact of pH is illustrated in Figure 7 for a test on 10 mm membrane (steel B) under 100 mbar $H_2S$ / 900 mbar $CO_2$, with successive pH steps from 5.5 to 2.8.

The impact of $H_2S$ partial pressure is illustrated in Figure 8, for permeation experiments on 1 mm thick membranes, tested at pH 5.5 with 0.3, 1 and 10 % $H_2S$ balanced with $CO_2$ to a total pressure of 1 bar.

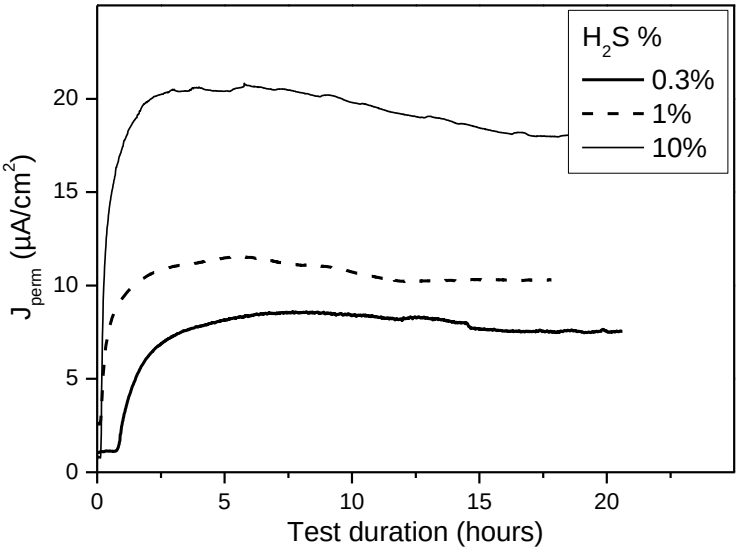


Figure 8: Permeation transients measured for 1 mm membranes of steel A exposed to test solution at pH 5.5 saturated under 1 bar with different $H_2S$ / $CO_2$ ratios.

As expected, the steady-state permeation flux increases with $H_2S$ partial pressure and with decreasing pH. In order to quantify the impact of both parameters, all the diffusion fluxes measured during this study were plotted in log scales as a function of $H_2S$ partial pressure (Figure 9) or as a function of pH (Figure 10).

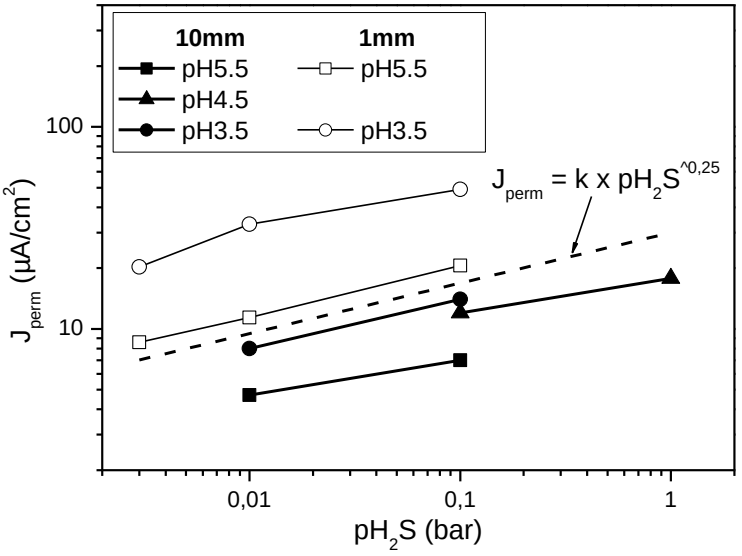


Figure 9: Evolution of the steady-state permeation flux with $H_2S$ partial pressure ($CO_2$ balance to 1 bar) for different pH and membrane thicknesses (steel B).

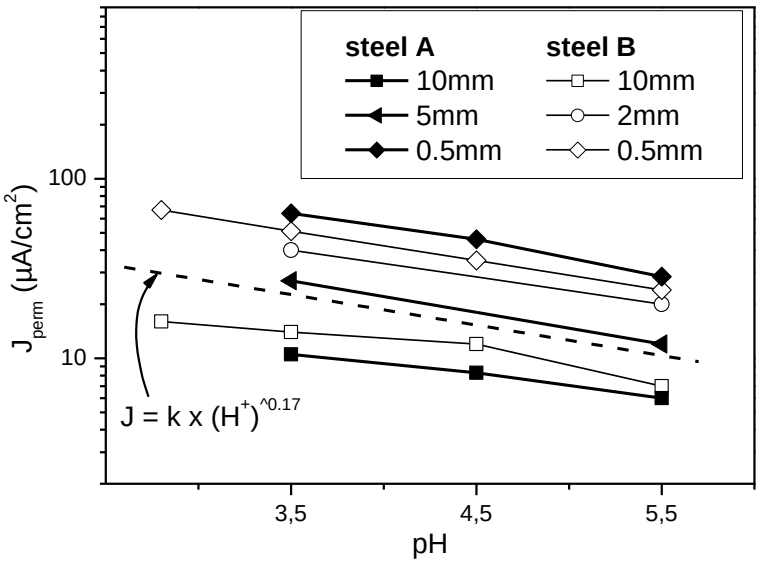


Figure 10: Evolution of the steady-state permeation flux with pH for experiments under 100 mbar $H_2S$ and 900 mbar $CO_2$, for different steel grades and different membrane thicknesses.

The same analysis was performed for the corrosion rate. For each experimental condition (pH – $pH_2S$), linear polarization measurements were made in the charging cell. The corresponding results are presented in Figure 11 for the influence of $H_2S$ partial pressure and in Figure 12 for pH. From Figure 11, representing the evolution of the corrosion current density with $H_2S$ partial pressure, it seems that the impact of $H_2S$ is greater at high pH. From Figure 12, we can see that the corrosion rates of steel A (sour service grade) always exceed those of steel B (sweet service grade). However, the impact of pH is quite similar for both steel grades.

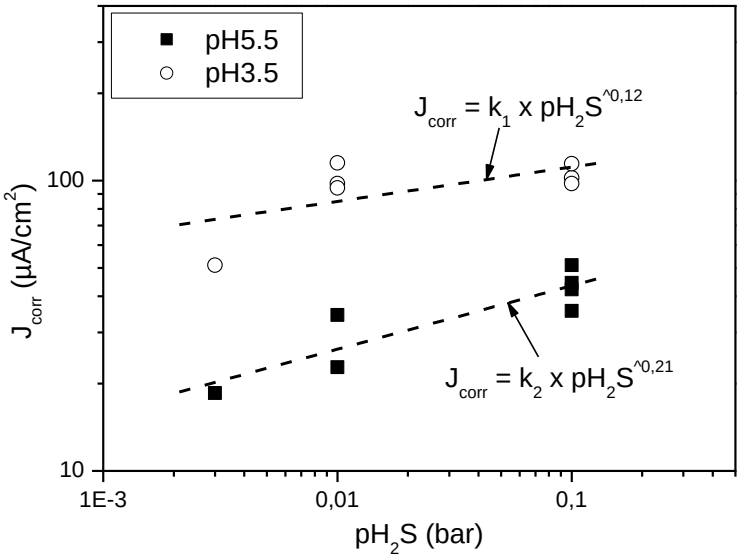


Figure 11: Evolution of the corrosion current density evaluated from Rp measurements as a function of $H_2S$ partial pressure ($CO_2$ balance to 1 bar) for different test solution pH (steel B).

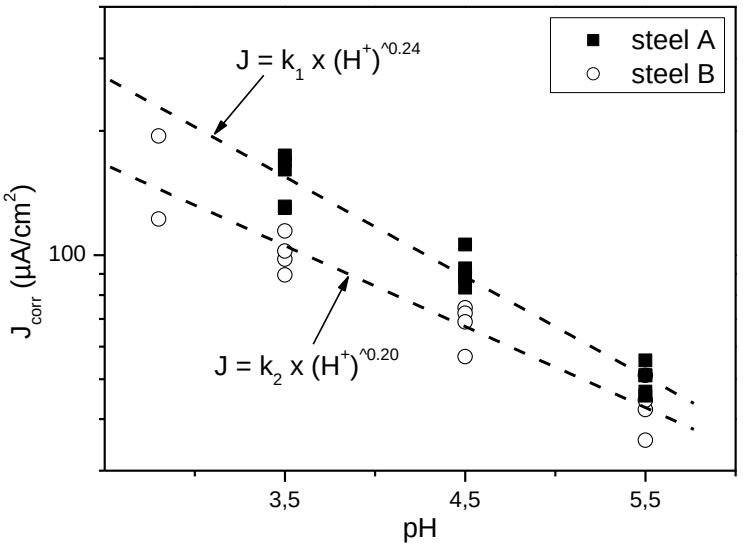


Figure 12: Evolution of the corrosion current density evaluated from Rp measurements as a function of pH and for experiments under 100 mbar $H_2S$ and 900 mbar $CO_2$, for different steel grades.

A unique expression could be derived to express the permeation flux evolution with proton concentration and $H_2S$ partial pressure:

$$J_{perm} \propto \left[H^+\right]^{0.17} \times \left[H_2S\right]^{0.25} \quad (19)$$

A law approximately similar was found for the corrosion rate, except that the pre-exponential factor was higher for steel grade A (higher corrosion):

$$J_{corr} \propto \left[H^+\right]^{0.20-0.24} \times \left[H_2S\right]^{0.12-0.21} \quad (20)$$

Quite remarkably, the exponential factor of the expression of the permeation flux with $H_2S$ partial pressure and $H^+$ concentration seems to be independent of the steel grade and of the membrane thickness. The comparison of these results with the literature is quite interesting. Asahi *et al.*[16] have studied low carbon high strength steels, and found that $J_{perm}$ was proportional to $\left(H^+ \times H_2S\right)^{0.25}$. A similar trend was observed by Boellinghaus *et al.*[36,37] for 13 % chromium martensitic martensitic stainless steels, with a steady state permeation flux proportional to $\left(H_2S\right)^{0.16-0.25}$. Those results were later confirmed by Duval *et al*.[34] for ARMCO iron membranes, with an expression very close to that obtained during the present study. They also performed the same analysis for corrosion rate, through linear polarization measurements:

$$J_{perm} \propto \left[H^+\right]^{0.25} \times \left[H_2S\right]^{0.15} \quad (21)$$

$$J_{corr} \propto \left[H^+\right]^{0.25} \times \left[H_2S\right]^{0.20} \quad (22)$$

These results, obtained on thin membranes (0.5 – 1 mm) are in good agreement with the results of the present study, with exponential factors between 0.15 and 0.25 for $H_2S$ and $H^+$ impacts on permeation and corrosion.

It is also extremely interesting to see that permeation on thick membranes still follows the same pH dependency than on thin membranes. More remarkable is the apparent absence of impact of the balance gas. Indeed, all the previous results[16,34,36,37] were obtained with $H_2S$ / $N_2$ gas mixtures, whereas $H_2S$ / $CO_2$ mixtures were used in the present work. This should give rise to completely different surface films. In the latter case, $HS^-$ adsorption is in competition with $HCO_3^-$, and a surface coverage of sulfide proportional to $HS^-/HCO_3^-$, i.e. proportional to $pH_2S/pCO_2$ is expected[53]. Then, the strict observance of the direct hydrogen charging model through $HS^-$

adsorbate would predict a $\left(pH_2S\right)^{\wedge 1}$ law[53]. According to Crolet[55] commenting the results of Asahi *et al*.[16], this dependence on $\left(H^+ \times H_2S\right)^{0.25}$ should result from an error bar in a reaction order of 0, rather than a really significant reaction order of ¼. New experiments in $H_2S$ / $N_2$ gas mix and comparisons with $H_2S$ / $CO_2$ mix should help clarifying this point.

**Impact of temperature**

The impact of temperature on corrosion and permeation was evaluated through experiments at pH 3.5 and under 10 % $H_2S$. The experimental cell was placed in an autoclave, and the temperature was progressively increased from 25 to 55 °C. A typical permeation transient is presented in Figure 13.

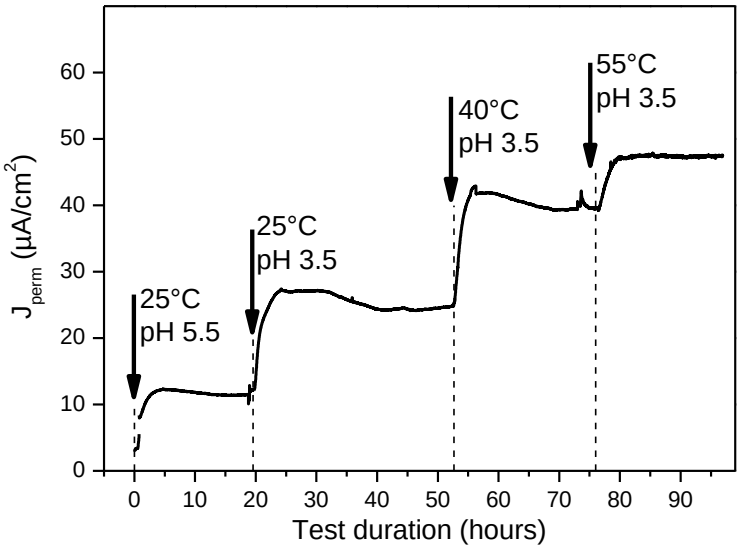


Figure 13: Impact of temperature on permeation transient measured for a 5 mm membrane of steel A exposed to test solution at various pH and under 100 mbar $H_2S$ and 900 mbar $CO_2$.

It has to be noted that gas saturation was always performed under atmospheric pressure: therefore, the partial pressure of $H_2S$ is not rigorously the same for all experiments, as the water partial pressure at 25°C is approximately 30 mbar, whereas it reaches 150 mbar at 55°C. Nevertheless, considering that the permeation flux for our experimental conditions can be well described with Equation (19), the deviation associated with the $H_2S$ partial pressure change between 25 °C and 55 °C would be less than 5 %.

In order to check if corrosion and permeation present thermal activation trends, the results are plotted in log scale, versus the reciprocal of temperature (Figure 14 and Figure 15).

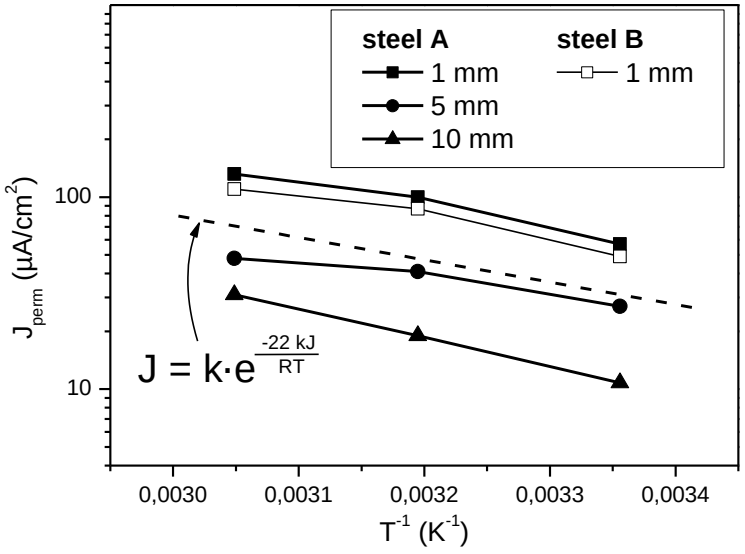


Figure 14: Evolution of the steady-state permeation flux with temperature, for different experiments at pH 3.5 under 10 % $H_2S$ and 90 % $CO_2$.

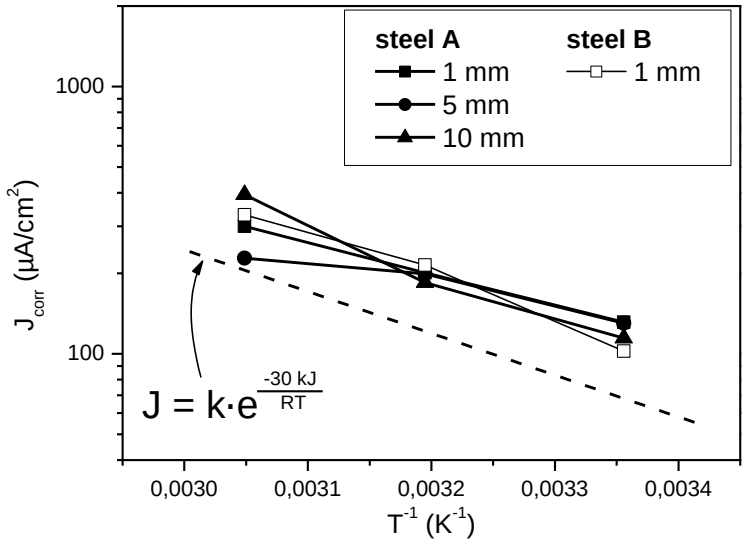


Figure 15: Evolution of the corrosion current with temperature, for different experiments at pH 3.5 under 10 % $H_2S$ and 90 % $CO_2$.

Within this range of temperature, the evolutions of $J_{corr}$ and $J_{perm}$ seem to follow an Arrhenius law:

$$J = J_0 \cdot e^{\frac{-E_a}{R \cdot T}} \tag{23}$$

The values of the corresponding activation energies $E_a$ are approximately 22 kJ.mol$^{-1}$ for the permeation flux and 30 kJ.mol$^{-1}$ for the corrosion rate.

The results are in good agreement with activation energies values found in the literature[14,61] for hydrogen diffusion coefficient, between 17 kJ.mol$^{-1}$ and 21 kJ.mol$^{-}$1. However, in the present study, only the diffusion flux was evaluated, and the individual contributions of the diffusion coefficient and of the sub-surface concentration of hydrogen could not be separated.

For corrosion rates in sour environment, no comparative results were found in the literature. The comparison with corrosion in $CO_2$ corrosion gave activation energies around 50 kJ.mol$^{-1}$ [62].

**Impact of Steel Membrane Thickness**

The impact of membrane thickness on permeation transient is illustrated in Figure 16, for permeation experiments on steel A membranes of various thickness, tested at pH 5.5 under 100 mbar $H_2S$ and 900 mbar $CO_2$.

As expected, the thickness increase resulted in a decrease in the steady-state permeation flux decreased and an increase in the breakthrough time.

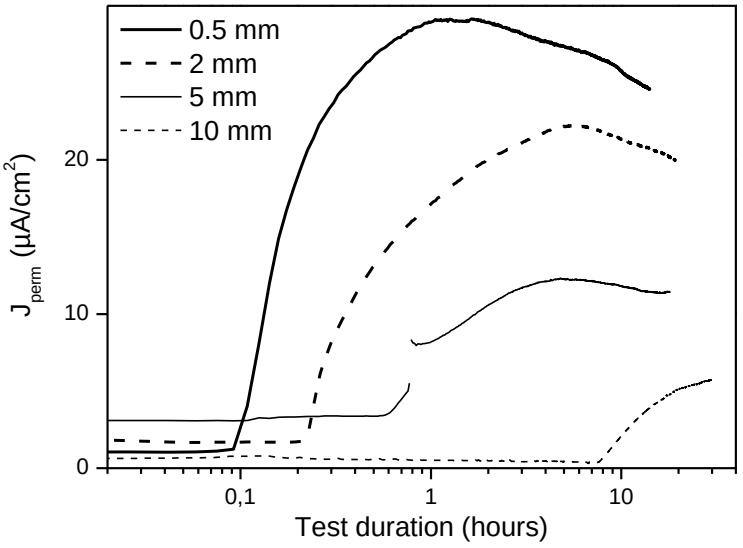


Figure 16: Permeation transients measured for steel A membranes of different thickness, exposed to test solution at pH 5.5 saturated with 100 mbar $H_2S$ and 900 mbar $CO_2$.

In order to verify the transition between thick and thin membrane behavior, the permeation flux was plotted versus the inverse of the membrane thickness, for tests under 100 mbar $H_2S$ and

900 mbar $CO_2$, at different pH and for both steel A and steel B (Figure 17). These experimental results accurately reproduce the theoretical predictions of Figure 2 [38,54], with a thin membrane region for which the permeation flux is independent of the membrane thickness, and a thick membrane region, where the linearity of the flux with the reciprocal of the thickness is verified (dashed lines on Figure 17). The expected transition at $d_{crit}$ is effectively observed, and occurred between 2 and 3 mm. Above this thickness, the permeation flux is inversely proportional to the membrane thickness. For thinner membrane, a constant flux is observed. These findings also confirm previous results of Duval *et al*.[34] who observed a thin membrane behavior up to 1.5 mm in comparable test solution. However, no clear demonstration of the transition between thick and thin membrane regimes was found in the literature to date.

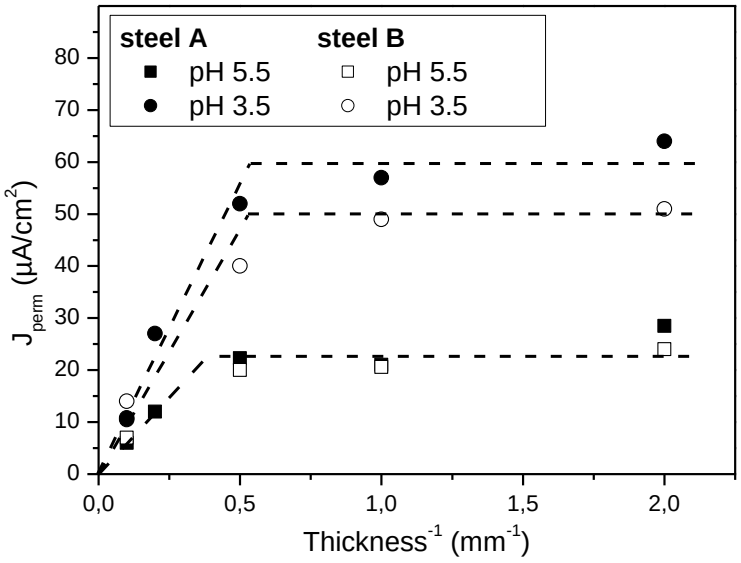


Figure 17: Evolution of the steady-state permeation flux with membrane thickness for different experiments under 100 mbar $H_2S$ and 900 mbar $CO_2$.

A more detailed interpretation of these results can be made after calculation of the permeation efficiency:

$$E_p = J_{diff} / J_{ch} \tag{24}$$

This ratio was calculated as follows. For a given experimental condition, *i.e.* same material, same pH and same $pH_2S$, the charging flux is constant and is given directly by the flux measured in a thin membrane condition, provided that the extraction method is ideal. Then, for each material and test solution (pH, $pH_2S$), the permeation efficiency was calculated for each thickness as the ratio between the diffusion flux divided by the diffusion flux measured for a 0.5 mm membrane. The corresponding results are presented in Figure 18, for tests on steel A and steel B, with pH from 2.8 to 5.5, and under 100 mbar $H_2S$ and 900 mbar $CO_2$.

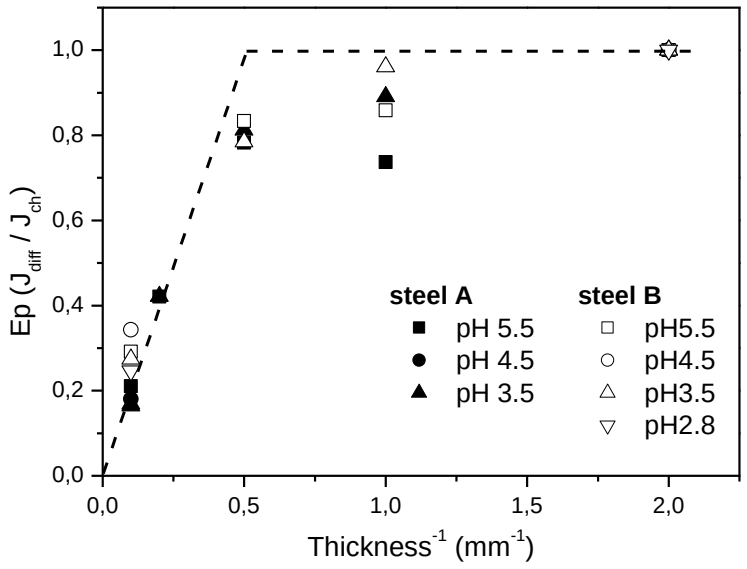


Figure 18: Evolution of permeation efficiency (Ep = $J_{diff}$ / $J_{ch}$) with membrane thickness, for all experiments under 100 mbar $H_2S$ and 900 mbar $CO_2$.

From this result, it is quite clear that for a given gas composition, the permeation efficiency has a similar shape, whatever the pH of the test solution between 2.8 and 5.5. The steel type does not seem to have an impact, but both had the same microstructure (ferrite - pearlite), steel A being sour service and steel B sweet service. This means that for a given $H_2S/CO_2$, any pH change will have the same quantitative impact on the charging flux $J_{ch}$ (equal to the diffusion flux measured on thin membrane) and on the hydrogen subsurface concentration $C_0$ (proportional to the diffusion flux measured on thick membrane). This could be explained by the fact that both the charging flux and the sub-surface concentration depend on the surface coverage of adsorbed hydrogen, which is strongly affected by the pH. Nevertheless this result was not straightforward in sour conditions, with ionic species at the steel surface acting as recombination poisons or hydrogen entry promoters. It would be extremely interesting to perform the same analysis for solutions with different $H_2S$ concentration. Then, it will be possible to compare the respective impact of pH and $pH_2S$ on SSC (presumably related to $J_{ch}$) and HIC (presumably related to $C_0$).

## CONCLUSION

The measurements performed during this study represent the first experimental evidence of the thin to thick membrane behavior for hydrogen diffusion in sour conditions. As already forecasted[34,54] the critical thickness corresponding to this transition is in the millimeter range, and does not seem to depend much on the test solution pH from 2.8 to 5.5. The impact of $H_2S$ was not quantified.

This result confirms the model proposed by Crolet[54] for the interpretation of permeation data of steel in sour conditions. Below the critical thickness, the diffusion flux $J_{diff}$ that is measured

corresponds to the charging flux $J_{ch}$, hence it may be expected to quantitatively relate to the severity of scenarios to cause SSC. Above the critical thickness, the diffusion flux is inversely proportional to the thickness and is therefore directly related to the sub-surface hydrogen concentration $C_0$ and hydrogen activity. This is one important parameter for the susceptibility of steel to HIC, though others are also thought to play a major role, such as the presence of particular species like MnS.

This suggests also that past studies on HIC or SSC of steels in sour conditions and under free-corroding conditions could have been misinterpreted. Indeed, many studies were made on steel membranes not thicker than 1 – 2 mm, which behave like thin membranes in $H_2S$ conditions. Then, the measured flux is constant and equal to the charging flux. It can therefore not be used for the determination of $C_0$, the result rather being an apparent sub-surface concentration $C^*$ proportional to the thickness and to the measured flux. Thus, the correlation with SSC that was sometimes found was a correct result, but the interpretation was wrong: the result of a thin membrane permeation measurement is proportional to the charging flux, and not to the sub-surface concentration. But SSC is related to the charging mechanism, and not to internal hydrogen concentration.

As a complement to the results obtained during this study, the determination of the permeation efficiency for various membrane thickness and for other $H_2S$ partial pressure would be of great interest: it would then be possible to study the pH – $pH_2S$ severity domains, for both HIC and SSC: the former in the light of permeation results on thick membranes, giving access to $C_0$, the latter in the light of permeation results on thin membranes, giving access to the charging flux $J_{ch}$.

## ACKNOWLEDGMENTS

The authors would like to thank Frank Dean, of Ion Science Ltd, for his kind assistance with the use of the Hydrosteel 7000 device.

The contribution of Gilbert Parrain for the measurements in $H_2S$ environments, and the comparisons between electrochemical and air stream permeation is also greatly acknowledged.

## REFERENCES

1. T.V.Bruno, C.Christensen, and R.T.Hill, "History and development of TM0284", Corrosion 1999, NACE Conf. Series, paper n°422 (1999)
2. T.Hara, H.Asahi, and H.Ogawa, "Conditions of hydrogen-induced corrosion occurrence of X65 grade line pipe steels in sour environments", Corrosion vol.60 n°12, 1113-1121 (2004)
3. R.D.Kane and M.S.Cayard, "NACE committee report 8X294: review of published litterature on wet H2S cracking", Corrosion 1999, NACE Conf. Series, paper n°420 (1999)
4. S.E.Mahmoud, C.W.Petersen, and R.J.Franco, "Overview of hydrogen induced cracking (HIC) of pressure vessels in upstream operations", Corrosion 1991, NACE Conf. Series, paper n°10 (1991)
5. E.M.Moore, "Hydrogen-induced damage in sour, wet crude pipelines", Journal of Petroleum Technology, 613-618 (1984)
6. S.N.Smith and M.W.Joosten, "Corrosion of carbon steel by H2S in CO2 containing oilfield environments", Corrosion 2006, NACE Conf. Series, paper n°115 (2006)
7. L.Smith, "An overview of european federation of corrosion documents EFC16 and EFC17", Corrosion 1999, NACE Conf. Series, paper n°423 (1999)

8. C.Bosch, J.P.Jansen, and T.Herrmann, "Fit-for-purpose HIC assessment of large diameter pipes for sour service application", Corrosion 2006, NACE Conf. Series, paper n°124 (2006)
9. S.Gerit, W.Bruckhoff, G.Schmitt, U.Pankoke, and B.Sadlowsky, "Influence of material properties and laboratory test conditions on SOHIC at line pipe carbon steels", Corrosion 1998, NACE Conf. Series, paper n°260 (1998)
10. T.Hara, H.Asahi, Y.Terada, T.Shigenobu, and H.Ogawa, "The condition of HIC occurence of X65 linepipe in wet H2S environments", Corrosion 1999, NACE Conf. Series, paper n°429 (1999)
11. T.Hermann, C.Bosch, and J.Martin, "HIC assessment of low alloy steel line pipe for sour service application - Literature survey", 3R International vol.44 n°7, 409-417 (2005)
12. J.Kittel, J.W.Martin, T.Cassagne, and C.Bosch, "Hydrogen induced cracking (HIC) - Laboratory testing assessment of low alloy steel linepipe", Corrosion 2008, NACE Conf. Series, paper n°110 (2008)
13. R.W.Revie, V.S.Sastri, G.R.Hoey, R.R.Ramsingh, D.K.Mak, and M.T.Shehata, "Hydrogen-Induced Cracking of Linepipe Steels .1. Threshold Hydrogen Concentration and pH", Corrosion vol.49 n°1, 17-23 (1993)
14. R.W.Revie, V.S.Sastri, M.Elboujdaini, R.R.Ramsingh, and Y.Lafrenière, "Hydrogen-induced cracking of line pipe steels used in sour service", Corrosion vol.49 n°7, 531-535 (1993)
15. G.P.Tiwari, A.Bose, J.K.Chakravartty, S.L.Wadekar, M.K.Totlani, R.N.Arya, and R.K.Fotedar, "A study of internal hydrogen embrittlement of steels", Materials Science and Engineering A-Structural Materials Properties Microstructure and Processing vol.286 n°2, 269-281 (2000)
16. H.Asahi, M.Ueno, and T.Yonezawa, "Prediction of sulfide stress cracking in high-strength tubulars", Corrosion vol.50 n°7, 537-545 (1994)

17. S.U.Koh, J.S.Kim, B.Y.Yang, and K.Y.Kim, "Effect of line pipe steel microstructure on susceptibility to sulfide stress cracking", Corrosion vol.60 n°3, 244-253 (2004)
18. J.Leyer, P.Sutter, H.Marchebois, C.Bosch, A.Kulgemeyer, and B.J.Orlans-Joliet, "SSC resistance of a 125 KSI steel grade in slightly sour environments", Corrosion 2005, NACE Conf. Series, paper n°88 (2005)
19. C.M.Liao and J.L.Lee, "Effect of Molybdenum on Sulfide Stress Cracking Resistance of Low-Alloy Steels", Corrosion vol.50 n°9, 695-704 (1994)
20. J.Marsh, "Comparing hydrogen permeation rates, corrosion rates and sulphide stress cracking resistance for C-110 and P-110 casing steel", Corrosion 2007, NACE Conf. Series, paper n°109 (2007)
21. C.Mendez, I.Martinez, L.Melian, and J.Vera, "Application of hydrogen permeation for monitoring sulfide stress cracking susceptibility", Corrosion 2002, NACE Conf. Series, paper n°342 (2002)
22. J.Mougin, M.S.Cayard, R.D.Kane, B.Ghys, and C.Pichard, "Sulfide stress cracking and corrosion fatigue of steels dedicated to bottom hole assembly components", Corrosion 2005, NACE Conf. Series, paper n°85 (2005)
23. K.E.Szklarz, "Sulfide stress cracking of a pipeline weld in sour gas service", Corrosion 1999, NACE Conf. Series, paper n°428 (1999)
24. L.W.Tsay, Y.C.Chen, and S.L.I.Chan, "Sulfide stress corrosion cracking and fatigue crack growth of welded TMCP API 5L X65 pipe-line steel", International Journal of Fatigue vol.23 n°2, 103-113 (2001)
25. C.Azevedo, P.S.A.Bezerra, F.Esteves, C.J.B.M.Joia, and O.R.Mattos, "Hydrogen permeation studied by electrochemical techniques", Electrochimica Acta vol.44 n°24, 4431-4442 (1999)

26. P.Bruzzoni, R.M.Carranza, J.R.C.Lacoste, and E.A.Crespo, "Hydrogen diffusion in alpha-iron studied using an electrochemical permeation transfer function", Electrochimica Acta vol.44 n°16, 2693-2704 (1999)
27. L.Coudreuse and J.Charles, "The use of a permeation technique to predict critical concentration of $H_2$ for cracking", Corrosion Science vol.27 n°10-11, 1169-1181 (1987)
28. M.A.V.Devanathan and Z.Stachurski, "The mechanism of hydrogen evolution on iron in acid solutions by determination of permeation rates", Journal of the Electrochemical Society vol.111 n°5, 619-623 (1964)
29. C.Gabrielli, G.Maurin, L.Mirkova, and H.Perrot, "Transfer function analysis of hydrogen permeation through a metallic membrane in a Devanathan cell - Part II: Experimental investigation on iron membrane", Journal of Electroanalytical Chemistry vol.590 n°1, 15-25 (2006)
30. M.Kimura, N.Totsuka, T.Kurisu, T.Hane, and Y.Nakai, "Effect of environmental factors on hydrogen permeation in line pipe steel", Corrosion vol.44 n°10, 738-744 (1988)
31. E.Lunarska, Y.Ososkov, and Y.Jagodzinsky, "Correlation between critical hydrogen concentration and hydrogen damage of pipeline steel", International Journal of Hydrogen Energy vol.22 n°2-3, 279-284 (1997)
32. G.T.Park, S.U.Koh, K.Y.Kim, and H.G.Jung, "Effect of steel microstructure on hydrogen permeation behavior and the determination of critical hydrogen flux for hydrogen embrittlement", Corrosion 2006, NACE Conf. Series, paper n°438 (2006)
33. J.R.Vera, R.Case, and A.Castro, "The relationship between hydrogen permeation and sulfide stress cracking susceptibility of OCTG materials at different temperatures and pH values", Corrosion 1997, NACE Conf. Series, paper n°47 (1997)
34. S.Duval, R.Antano-Lopez, C.Scomparin, M.Jerome, and F.Ropital, "Hydrogen permeation through ARMCO iron membranes in sour media", Corrosion 2004, NACE Conf. Series, paper n°740 (2004)

35. S.U.Koh, B.Y.Yang, and K.Y.Kim, "Effect of alloying elements on the susceptibility to sulfide stress cracking of line pipe steels", Corrosion vol.60 n°3, 262-274 (2004)
36. T.Boellinghaus, H.Hoffmeister, J.Klemme, and H.Alzer, "Hydrogen permeation in a low carbon martensitic stainless steel exposed to H2S containing brines at free corrosion", Corrosion 1999, NACE Conf. Series, paper n°609 (1999)
37. T.Boellinghaus and H.Hoffmeister, "hydrogen permeation in supermartensitic stainless steels dependent on heat treatment and chemical composition", Corrosion 2000, NACE Conf. Series, paper n°141 (2000)
38. M.R.Bonis and J.L.Crolet, "Permeation measurments on thin steel membranes", Corrosion 2002, NACE Conf. Series, paper n°36 (2002)
39. F.W.H.Dean and D.J.Fray, "Ultrasensitive technique for detection of hydrogen emanating from steel and other solid surfaces", Materials Science and Technology vol.16, 41-46 (2000)
40. F.W.H.Dean and S.W.Powell, "hydrogen flux and high temperature acid corrosion", Corrosion 2006, NACE Conf. Series, paper n°436 (2006)
41. A.D.Ethridge, E.B.McDonald, D.G.Serate, and F.W.H.Dean, "Examples of use and interpretation of field data using a portable hydrogen permeation monitor", Corrosion 2004, NACE Conf. Series, paper n°477 (2004)
42. F.W.H.Dean, M.J.Caroll, and P.A.Nutty, "Hydrogen permeation flux data correlation with in-line corrosion monitoring techniques mapped over location and time", Corrosion 2001, NACE Conf. Series, paper n°636 (2001)
43. R.D.Tems and F.W.H.Dean, "Filed application of a new, portable, non-intrusive hydrogen monitor for sour service", Corrosion 2000, NACE Conf. Series, paper n°471 (2000)
44. F.W.H.Dean and S.W.Powell, "A laboratory study of types of corrosion inducing hydrogen permeation through steel", Corrosion 2004, NACE Conf. Series, paper n°472 (2004)

45. F.W.H.Dean, "Measurement of hydrogen permeation through structural steel sections of varying thickness at 19 degrees C", Materials Science and Technology vol.21 n°3, 347-351 (2005)
46. S.J.Mishael, F.W.H.Dean, and C.M.Fowler, "Practical applications of hydrogen permeation monitoring", Corrosion 2004, NACE Conf. Series, paper n°476 (2004)
47. J.O.Bockris, J.McBreen, and L.Nanis, "The hydrogen evolution kinetics and hydrogen entry into a-iron", Journal of the Electrochemical Society vol.112 n°10, 1025-1031 (1965)
48. R.N.Iyer, H.W.Pickering, and M.Zamanzadeh, "Analysis of hydrogen evolution and entry into metals for the discharge-recombination process", Journal of the Electrochemical Society vol.136 n°9, 2463-2470 (1989)
49. R.N.Iyer, I.Takeuchi, M.Zamanzadeh, and H.W.Pickering, "Hydrogen sulfide effect on hydrogen entry into iron - A mechanistic study", Corrosion vol.46 n°6, 460-468 (1990)
50. P.Marcus ed., "Corrosion Mechanisms in Theory and in Practice", 2nd edition (Marcel Dekker Inc. 2002), chapter n°3, 53-96 (2002)
51. ASTM G148-97 (revised 2003) "Standard practice for evaluation of hydrogen uptake, permeation, and transport in metals by an electrochemical technique"
52. J.Crank, "The mathematics of diffusion", 2nd edition, Oxford University Press Inc. (1975)
53. J.L.Crolet and G.Maisonneuve, "Construction of a universal scale of severity for hydrogen cracking", Corrosion 2000, NACE Conf. Series, paper n°127 (2000)
54. J.L.Crolet and M.R.Bonis, "Revisiting hydrogen in steel, part I: theoretical aspects of charging, stress cracking and permeation", Corrosion 2001, NACE Conf. Series, paper n°67 (2001)
55. J.L.Crolet and M.R.Bonis, "Revisiting hydrogen in steel, part II: experimental verifications", Corrosion 2001, NACE Conf. Series, paper n°72 (2001)

56. EFC publication n°16, "Guidelines on materials requirements for carbon and low alloy steels for $H_2S$-containing environments in Oil and Gas production", The Institute of Materials, London, UK (1995)
57. P.Manolatos and M.Jerome, "A thin palladium coating on iron for hydrogen permeation studies", Electrochimica Acta vol.41 n°3, 359-365 (1996)
58. P.Manolatos, M.Jerome, C.Duret-Thual, and J.Le Coze, "The electrochemical permeation of hydrogen in steels without palladium coating. Part I: Interpretation difficulties", Corrosion Science vol.37 n°11, 1773-1783 (1995)
59. P.Manolatos, M.Jerome, and J.Galland, "Necessity of a palladium coating to ensure hydrogen oxidation during electrochemical permeation measurements on iron", Electrochimica Acta vol.40 n°7, 867-871 (1995)
60. M.A.Veloz and I.Gonzalez, "Electrochemical study of carbon steel corrosion in buffered acetic acid solutions with chlorides and $H_2S$", Electrochimica Acta vol.48 n°2, 135-144 (2002)
61. F.W.H.Dean, T.M.Smeeton, and D.J.Fray, "Hydrogen permeation through mild steel in temperature range 20-500°C measured by hydrogen collection method", Materials Science and Technology vol.18 n°8, 851-855 (2002)
62. EFC publication n°13, "Predicting $CO_2$ corrosion in the oil & gas industry", The Institute of Materials, London, UK (1994)